Applied Physics A (2018) 124:485
https://doi.org/10.1007/s00339-018-1894-9

Applied Physics A
Materials Science & Processing

Facile solvothermal synthesis of $ZnCo_2O_4/MnO_2$ nanosheets composite with enhanced electrochemical properties as supercapacitor electrodes

Huanhuan Li[1] · Lei Wang[1] · Yuming Guan[1] · Yibo Su[1] · Jingbo Mu[1] · Hongwei Che[1] · Aifeng Liu[1] · Zengcai Guo[1]

Received: 5 April 2018 / Accepted: 2 June 2018 / Published online: 11 June 2018

Abstract

The $ZnCo_2O_4/MnO_2$ nanosheets composite is prepared through a facile solvothermal method. It is shown that the $ZnCo_2O_4/MnO_2$ electrode can exhibit a higher capacity of 286 F/g in three-electrode systems. Moreover, an asymmetric supercapacitor (ASC) is fabricated, in which the as-prepared $ZnCo_2O_4/MnO_2$ and active carbon are used as the positive and negative electrodes, respectively, delivering a maximum energy density of 16.94 W h/kg (based on the total materials' mass of two electrodes, at a power density of 750 W/kg) and an excellent specific capacity of 54.2 F/g. The exceptional retention of 98.5% initial capacitance is obtained after 1500 cycles. This ASC's practical energy-storage is demonstrated by light a LED belt when two such setups are charged. Thus, these excellent electrochemical performances make the composite hold great potential for next-generation supercapacitor applications.

Graphical abstract

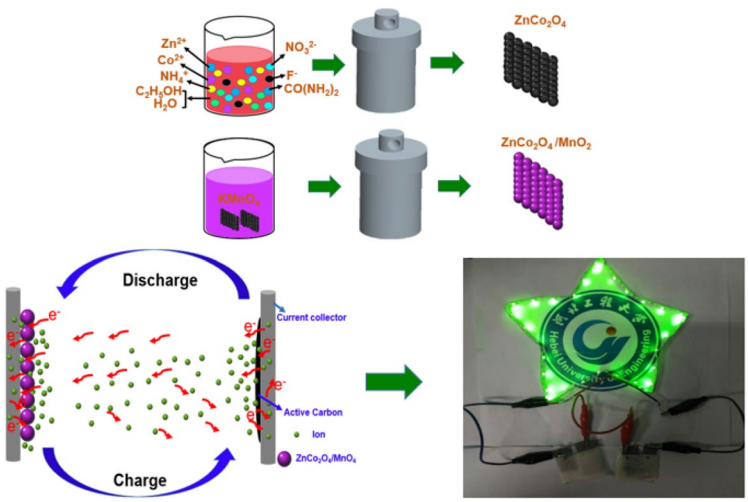

1 Introduction

Nowadays, with environmental pollution getting more serious, the development of clean, environment-friendly and sustainable energy is imminent. Super-capacitors (SCs), as one of advanced energy storage devices, have attracted unprecedented research boom. They combine the strong points of dielectric capacitor and rechargeable battery, which

✉ Jingbo Mu
jingbomu@hebeu.edu.cn

✉ Zengcai Guo
guozengcai@sina.com

[1] Institute of Novel Materials for Energy and Environment, College of Materials Science and Engineering, Hebei University of Engineering, Handan 056038, People's Republic of China

can deliver superior power and energy. SCs have two main types by their working mechanism: the electrical double-layer capacitors can store charges by charge separation; and the pseudo-capacitors, which offer a much higher specific capacitance, benefit from the reversible faradic reactions [1–3]. Compared to the former, the electrode materials of pseudo-capacitors have been strong concerned due to their enhanced capacitance and excellent electrochemical behavior. It is well known that metal oxides are commonly used as pseudo-capacitor electrode materials.

Among various metal oxides, $ZnCo_2O_4$ has attracted a special attention, due to its unique cubic spinel structure. The Zn^{2+} and Co^{3+} occupy the tetrahedral and octahedral positions, respectively, forming a multivalent state, and the electron transporting activity can be reduced. This is an outstanding electronic conductivity of $ZnCo_2O_4$ compared with single metal oxides (cobalt oxide and zinc oxide) [4]. The special structure of $ZnCo_2O_4$ leads to stronger electrochemical activities, higher electron transport capacity and richer redox reactions, which enables $ZnCo_2O_4$ to be one of the most promising electrode materials [5]. However, $ZnCo_2O_4$ limits application on high-performance devices due to the low specific capacity as well as rapid capacity-fading caused by repeated charge and discharge. Thus, seeking out a rational design and suitable material to improve $ZnCo_2O_4$'s capacity is generally regarded as an effective method.

As is well known, MnO_2 has been widely used as an ideal electrode active material owing to its superior electrochemical activity and high theoretical capacity (about 1370 F/g), as well as other advantages, such as low cost, environmental friendliness and abundant natural resources. Hence, various MnO_2 based composite electrode materials were obtained, in which MnO_2 was used to improve the specific capacitance of the composite electrode [6–10]. However, the poor conductivity of MnO_2 limits its practical application on high-performance energy storage devices [11–13]. Recently, two-dimensional (2D) nanomaterials, particularly ultrathin nanosheets with the thickness of several nanometers, have generated considerable interest in the field of energy storage due to their unique properties [14, 15]. Generally, the ultrathin 2D nanomaterials are nearly made up of surfaces with molecular-scale thickness, causing a high percentage of surface atoms and high efficient active sites on the exposed surface. The unique structure and surface properties of the ultrathin 2D nanomaterials make them more attractive in energy devices. More importantly, the ultrathin 2D nanostructures can provide short ion and electron diffusion path distances, large electrochemical active sites and electrode–electrolyte interface, high electronic conductivity, and improved structural stability [16, 17].

Based on the above analysis, it can be an ideal design to combine the merits of $ZnCo_2O_4$ and MnO_2, which produces a hopeful electrode material for high performance supercapacitor. Hence, $ZnCo_2O_4/MnO_2$ nanosheets are constructed by solvothermal method. In this system, $ZnCo_2O_4$ is considered as an excellent conductive substrate covered by MnO_2. Moreover, the nanosheets structure can provide more active sites that contribute to the attachment of MnO_2, offering fast transmission channels for electron. MnO_2 can improve the whole capacity, the synergetic effect between $ZnCo_2O_4$ and MnO_2 result in that the entire system has excellent electrochemical performance.

2 Experimental

2.1 Preparation of $ZnCo_2O_4$ precursor

$ZnCo_2O_4$ precursor were prepared by a facial solvothermal method. Typically, put 5 mmol $Co(NH_2)_2$, 1 mmol $ZnCo_2O_4{\cdot}6H_2O$, 2 mmol $Co(NO_3)_2{\cdot}6H_2O$, 2 mmol NH_4F and 30 mL ethyl alcohol sequentially into 45 mL deionized water, and stirred to a pink solution. Then, transferred the solution into four 25 ml Teflon-lined and heated to 140 °C for 4 h, dried after washing several times with deionized water. Subsequently, under the protection of N_2, heated it at 400 °C for 4 h and then $ZnCo_2O_4$ precursor is obtained.

2.2 Synthesis of $ZnCo_2O_4/MnO_2$ nanosheets composites

$ZnCo_2O_4/MnO_2$ composites were fabricated by taking three samples of $ZnCo_2O_4$ precursor, and, respectively, added in 0.063, 0.031, 0.015 g $KMnO_4$ and 20 mL deionized water solutions. Stirred for 10 min and heated to 160 °C for 2 h in Teflon-lined. Finally, the samples were washed and dried at room temperature. We have separately sorted these three samples as ZM-1, ZM-2, ZM-3, respectively. Detailed preparation process was presented in Fig. 1.

2.3 Materials characterization

The samples' microstructure was conducted through a FEG 250 field-emission scanning electron microscope (SEM) system (FEI Co., Hillsboro, OR, USA) and further obtained using a JEM 2100F transmission electron microscopy (TEM). The TEM was made by JEOL Ltd., Tokyo, Japan and accelerated to a voltage of 200 kV. The material's crystal structure was measured via powder X-ray diffraction (XRD) patterns with Cu-Kα radiation 10–70°. X-ray photoelectron spectrometer (XPS) was characterized to investigate the chemical structure of the samples (VG Scientific ESCALAB LK II spectrometer; Thermo Fisher Scientific Inc., Waltham, MA, USA).

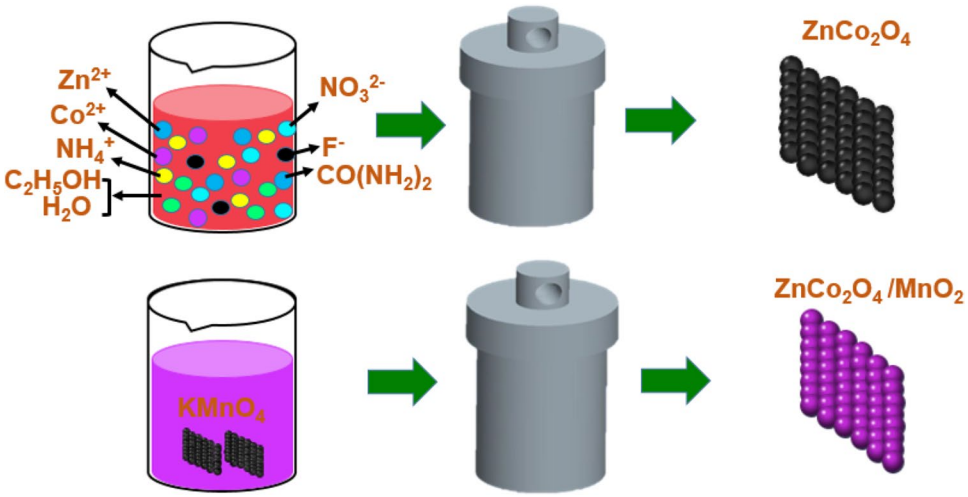

Fig. 1 Preparation process for the $ZnCo_2O_4/MnO_2$ nanosheets composites

2.4 Fabrication of an ASC

To fabricate an ASC device, ZM-2 and active carbon (AC) were used as positive and negative electrodes of supercapacitor, respectively. Active materials (ZM-2/AC) loading mass ratio was determined by the charge balance relationship of $q^+ = q^-$. Typically, q^+ and q^- were used to represent the electrode charges. The mass balance of composite aimed to meet $q^+ = q^-$, which depended on the following equation [18–21]:

$$q = m \times C \times \Delta V \tag{1}$$

$$m^+/m^- = (C^- \times \Delta V^-)/(C^+ \times \Delta V^+) \tag{2}$$

where m (g), C (F/g) and ΔV (V) represent the active material mass, the electrode specific capacitance, and the operating voltage, respectively. And the specific capacity Cs could be calculated according to the following equation:

$$Cs = I \Delta t / (m \Delta V) \tag{3}$$

where I, Δt, m, ΔV represent the power current, the discharge time, the total mass of working electrode and operating voltage window, respectively.

2.5 Electrochemical measurements

All the electrochemical performances were tested by a CHI 660E electrochemical workstation (Shanghai Chenhua Co. Ltd, China), and 6M aqueous KOH solution was treated as electrolyte. In the three-electrode system, galvanostatic charge and discharge, cyclic voltammetry and electrochemical impedance spectroscopy (EIS) were measured. $ZnCo_2O_4/MnO_2$, platinum wire and Hg/HgO were, respectively, used as a working electrode, a counter electrode and a reference electrode. Based on a weight ratio of 8/1/1, mixed $ZnCo_2O_4/MnO_2$ composite, acetylene black and polyvinylidene fluoride binder ethanol mixture to make working electrodes and then pressed onto nickel foam current collectors, dried at 353 K for 12 h [22–24].

3 Results and discussions

The $ZnCo_2O_4/MnO_2$ nanosheets' morphologies were measured via a scanning electron microscopic (SEM). Figure 2a showed the structure of ZM-1 composite, it could be clearly seen that composite was nanosheet composed of nanoparticles, and the thickness was about 30 nm, the over-all structure relative loose or even collapsed. The morphology of ZM-2 was presented in Fig. 2b, comparing with the ZM-1, the nanosheet structure of ZM-2 became more compacted and denser. It was clear that ZM-2 nanosheets' thickness was increased to 50 nm. The nanosheets were well covered by MnO_2 and the structure was also accumulated of nanoparticles, providing other transmission channels for ions and electrons. With increasing MnO_2 loading, the structure of ZM-3 nanosheets composite was displayed in Fig. 2c, the surface became rougher than former due to the increasing of MnO_2. The nanoparticles on the surface of nanosheets had gradually agglomerated. What's more, the nanosheets had been severely damaged.

To further analyze the nanosheets' composition and morphology, ZM-1 and ZM-2 composite took transmission electron microscopy (TEM) and high-resolution TEM (HRTEM) observations. Figure 3a was the TEM image of ZM-1 nanosheet, it could be clearly seen that the nanosheet was constructed by loosen nanoparticles. HRTEM image of ZM-1 was shown in Fig. 3b, which displayed two types of clear lattice fringes, the fringes spacing was ca. 0.241, corresponding to the crystal structure of $ZnCo_2O_4$, and another set of the clear fringes spacing measure ca. 0.237 nm, which

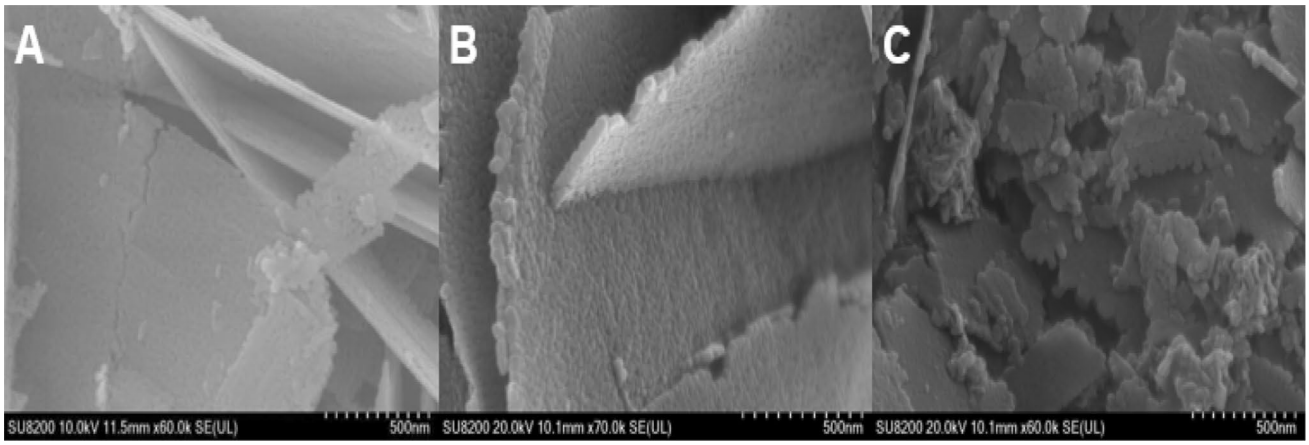

Fig. 2 SEM images of samples **a** ZM-1, **b** ZM-2 and **c** ZM-3 at same magnification

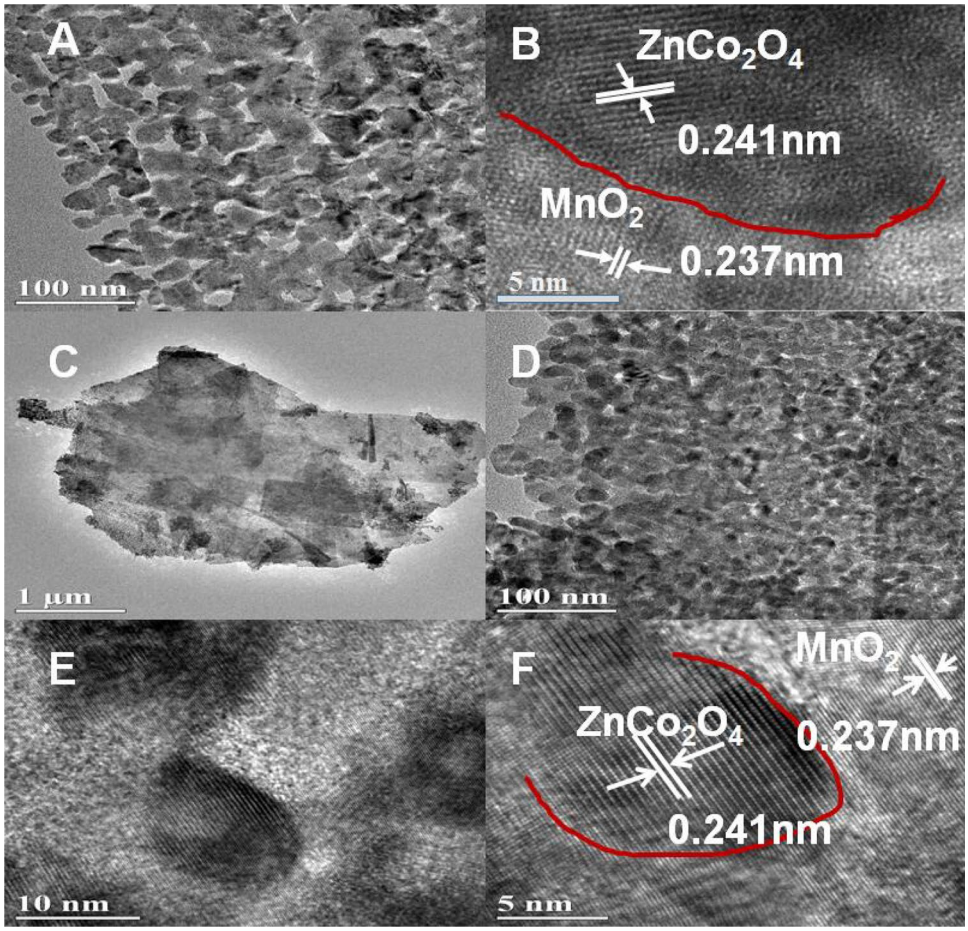

Fig. 3 **a, b** TEM and HRTEM images of ZM-1 nanosheets composite; **c–f** TEM and HRTEM images of ZM-2 nanosheets composite

corresponded to the lattice spacing of the MnO_2. Figure 3c showed that ZM-2 composite exhibited a geometrical sheet-like 2D structure. Figure 3d further revealed the structure of $ZnCo_2O_4/MnO_2$ composite, the nanosheets was constructed by nanoparticles and well combined with MnO_2 nanoparticles uniformly, the TEM images were in good agreement with the SEM analysis in Fig. 2. From Fig. 3e, f, it was very easy to see clear lattice stripes and an obviously grain boundary. In Figure E. The crystal lattice spacings were 0.241 and 0.237 nm, which corresponded to the (311) (211) crystal planes of α-MnO_2 and $ZnCo_2O_4$ crystals, respectively [25, 26].

The composition, internal structure and morphology of fabricated composite were detected by X-ray diffraction (XRD). From the patterns of Fig. 4, the main diffraction peaks of $ZnCo_2O_4$ (JCPDS card no. 81-2299) were found in composite material, and the diffraction peak about $2\theta = \sim 36.5$ correspond well to the (311) planes of $ZnCo_2O_4$. Meanwhile, all MnO_2 diffraction peaks were well indexed to reflection peaks that consistent with the α-MnO_2 (JCPDS card no. 44–141). Furthermore, the peak of $2\theta = \sim 37.0$ was found that indexing MnO_2's (211) planes [27, 28]. The characteristic peaks of MnO_2 and $ZnCo_2O_4$ could indicate the nanosheets of $ZnCo_2O_4/MnO_2$ composite were successfully synthesized.

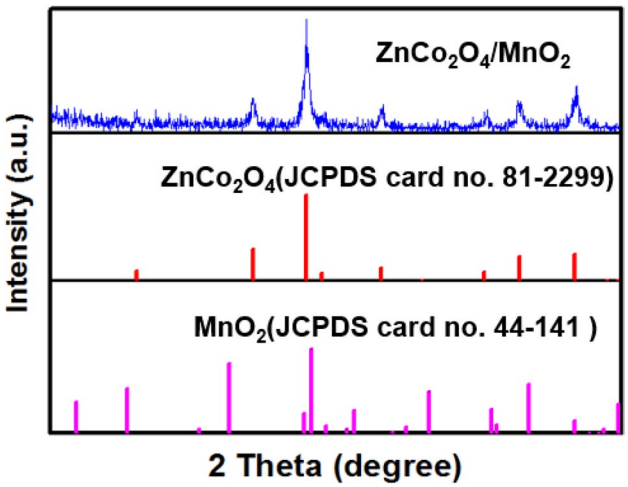

Fig. 4 The XRD patterns of $ZnCo_2O_4/MnO_2$ composite with pure $ZnCo_2O_4$ and MnO_2

The bonding configuration and chemical composition of the $ZnCo_2O_4/MnO_2$ nanosheets composites were analyzed through X-ray photoelectron spectroscopy (XPS). Figure 5a shown the fully scanned spectra of XPS that Mn, Zn, O, Co, C were determined, certificating the chemical components of $ZnCo_2O_4/MnO_2$. To reveal the elemental valence, the peaks in 641.7 and 653.5 eV in Fig. 5b corresponded to Mn $2p_{3/2}$ and Mn $2p_{5/2}$, respectively, demonstrating existence of Mn^{4+} of MnO_2. The amplified spectrum of Zn in Fig. 5c showed two strong characteristic peaks at 1021 and 1044 eV, pointing to Zn $2p_{3/2}$ and Zn $2p_{1/2,}$ to explain the presence of Zn^{2+}. In Fig. 5d, the enlarged spectra O 1 s was further demonstrated two characteristic peaks pointing to oxygen species of $ZnCo_2O_4$ and MnO_2, the peaks at 529.6 and 531.3 eV were attributed to the O^{2-} forming oxide with cobalt and manganese elements, respectively. All above testing methods were to illustrate the formation of $ZnCo_2O_4/MnO_2$ composite [29–32].

The electrochemical performance of samples was investigated through Galvanostatic charge–discharge (GCD) and Cyclic voltammograms (CV) via a three-electrode configuration test, which made 6 M KOH solution as the electrolyte.

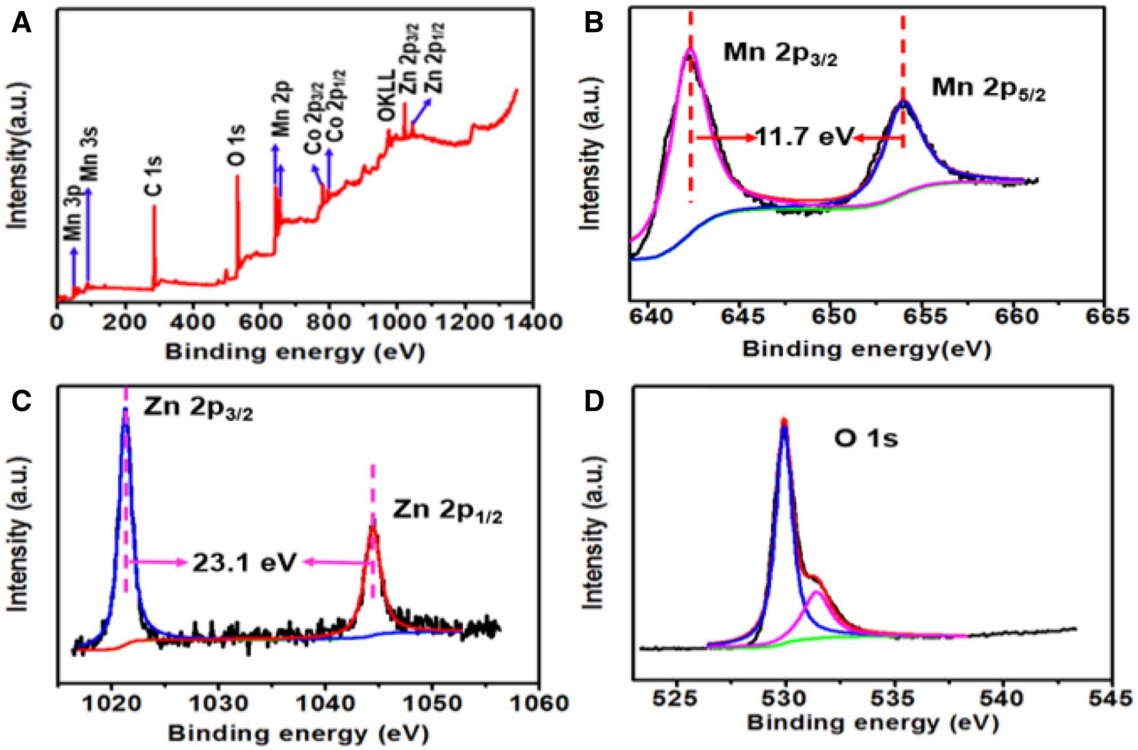

Fig. 5 **a** XPS fully scanned spectra of $ZnCo_2O_4/MnO_2$. **b** Mn 2p scan **c** Zn 3p scan and **d** O 1 s scan

The CV curves reflected the stability of electrode materials and the curve area represented the specific capacitance. Obviously, in Fig. 6a, all the CV curves exhibited well-defined redox peaks which were very different from the Electric Double-Layer Capacitance (EDLC). After adding MnO_2, the composite materials had strong pseudo-capacitive behavior due to a pair of obvious redox peaks at ~0.28 and ~0.37 V. It could be found that pure $ZnCo_2O_4$ had relatively weak response current, indicating that MnO_2 indeed increased the capacitance of $ZnCo_2O_4$ electrode. The redox peaks of composite shifted because the rich pseudo-capacitive reaction of the Mn^{4+}/Mn^{3+} and $Co(OH)_2/CoOOH$ redox couples [33, 34]. The symmetrical curves of GCD implied excellent reversible behavior. According to the Eq. (3), we obtained samples' capacitance 230, 286, 280, 190.6 F/g in Fig. 6b, respectively. From ZM-1, ZM-2 and ZM-3, capacity changes can be drawn, the capacity of $ZnCo_2O_4$ does not increase in proportion to the load of MnO_2. ZM-3 capacity reduction might be due to the MnO_2 agglomeration, and the load of MnO_2 should had the best conditions. The proper content of MnO_2 would make sure that the electrode material had a better electrochemical performance, and excessive MnO_2 could lead to the reduction of effective area with which electrolyte is in contact.

Moreover, a series of electrochemical measurements were performed to investigate the electrochemical properties of the electrode. The samples' charge–discharge and cyclic voltammetry performance were separately tested at different current densities and sweep rates. Figure 7a, c, and e showed the CV performance and Figure b, d, and f exhibited the GCD curves of the samples respectively. Figure 7a showed the curves shape of ZM-1 was not significantly influenced by the increasing of scan rates. It indicated that the electron conduction improved and the electrochemical performance in the materials was very stable. Figure 7b revealed that the curves of ZM-1 remained symmetrical when density increased. It was clearly shown that ZM-2 nanosheets composite had a steady voltage of 0.5 V at different scan rates, ranging from 5 to 100 mV/s as shown in Fig. 7c. At a scan rate of 5 mV/s, the strong faradaic reaction generated the anodic peak lay near 0.28 V and the cathode peak lay around 0.37 V, revealing the mechanism of energy storage. In addition to its stable properties, with the scan rate increasing, the anodic/cathodic peak, respectively, shifted toward positive/negative potential due to the kinetic irreversibility during the faradaic process in $ZnCo_2O_4/MnO_2$ composite. At changeable current density ranging from 1 to 10 A/g, Fig. 7d based on Eq. (3), shown that the ZM-2 composites' specific capacity varies from 286 to 176 F/g. The total capacitive increase of $ZnCo_2O_4/MnO_2$ electrode may be attributed to the dominant contribution of the nanosheet structure, providing the faraday reaction with sufficient active sites and channels for rapid transportation of electrons/ions. From Fig. 7e, ZM-3 area decreased in comparison to ZM-2 composite. Figure 7e was consistent with the calculation results of Fig. 7f. From the above analysis, it was shown that the suitable load of MnO_2 in ZM-2 possessed the best electrochemical performance and stability [35].

The specific capacitance of ZM-1, ZM-2, ZM-3 and $ZnCo_2O_4$ electrodes were tested in Fig. 8a. The specific capacitance reduced with the current density enhancing. The ZM-2 electrode exhibited higher capacity than other samples' results through in comparison with the various electrode types. Meanwhile, the capacitance of the ZM-2 composite material accounted for 61.53% of the initial capacitance. The electrochemical performance was further investigated by an electrochemical impedance spectroscopy in Fig. 8b to test the kinetic properties of electrode materials. The three electrodes displayed a similar curve-form, in which the intercept with the real axis represented the equivalent series resistance (R_e), the semicircular area in high frequency equivalent to charge transfer resistance (R_{ct})

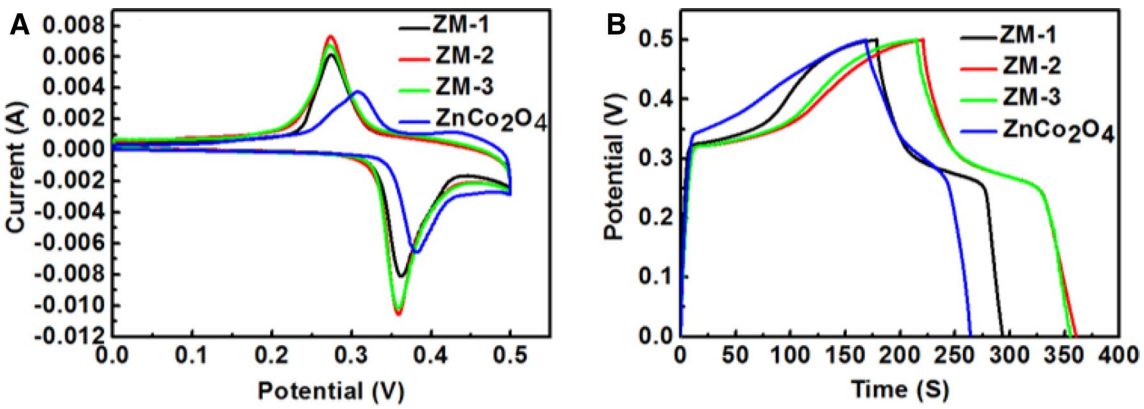

Fig. 6 **a** Cyclic voltammograms curves of ZM-1, ZM-2, ZM-3 and pure $ZnCo_2O_4$ electrodes at a scan rate of 5 mV/s. **b** Galvanostatic charge–discharge curves of the ZM-1, ZM-2, ZM-3 and $ZnCo_2O_4$ at 1 A/g

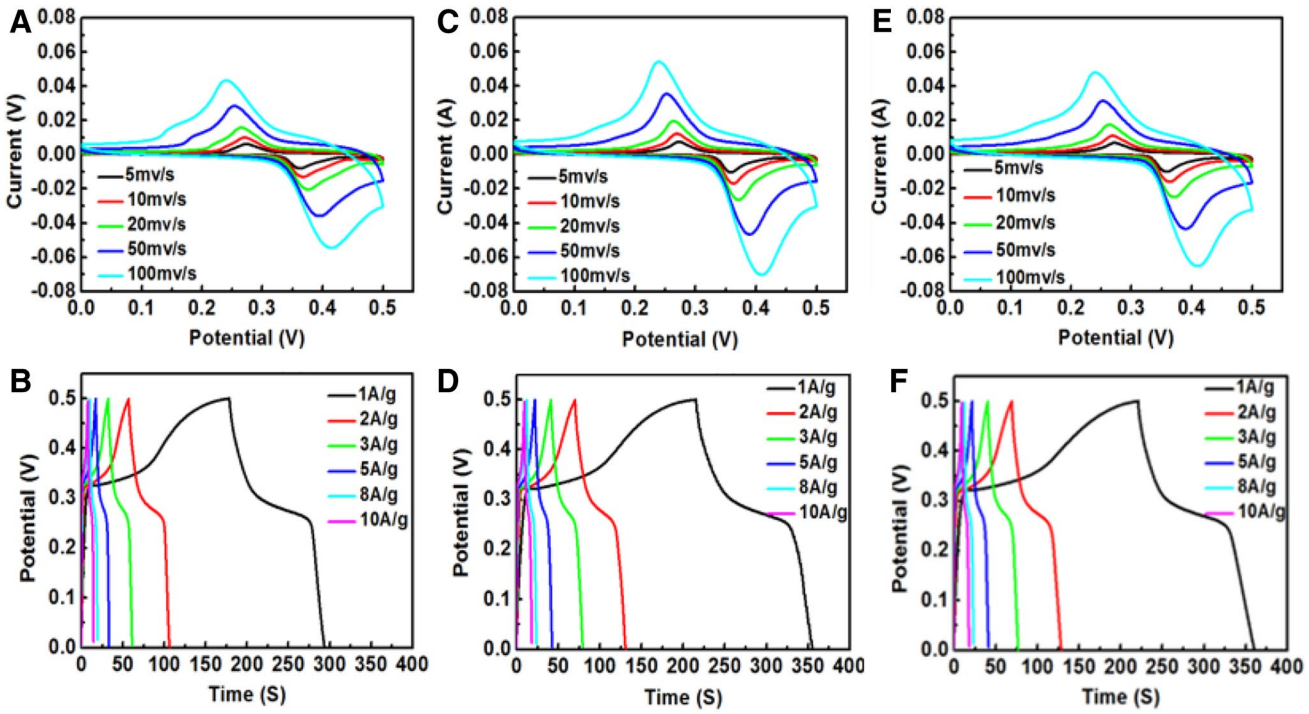

Fig. 7 The cyclic voltammograms and galvanostatic charge–discharge curves of ZM-1 (**a, b**), ZM-2 (**c, d**), ZM-3 (**e, f**) at different scan rates and densities in 6M KOH solution

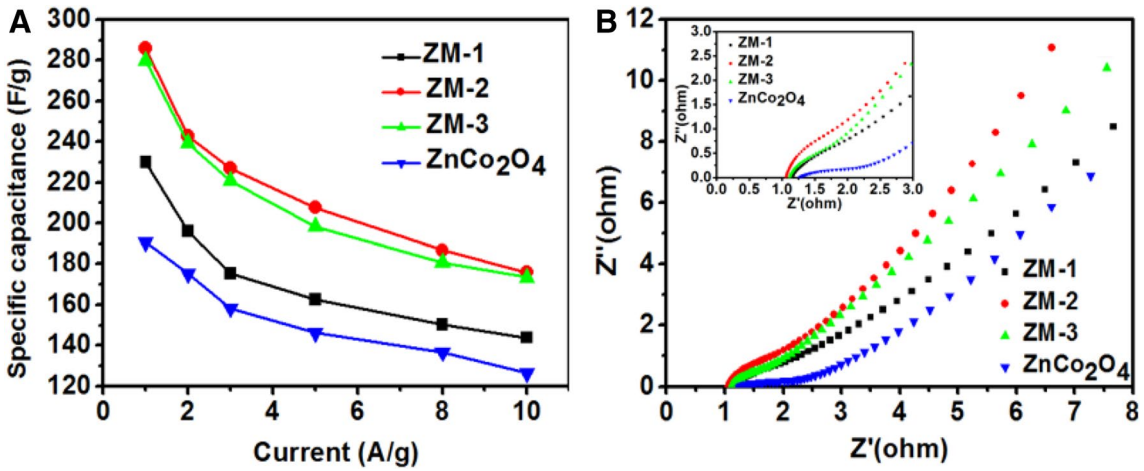

Fig. 8 **a** Specific capacitance for all obtained samples at different densities of 1–10 A/g and the electrochemical impedance spectroscopy (EIS) in (**b**)

and the low-frequency area line showed the rate capability of the composite. Based on samples' comparison, the line of ZM-2 at low frequency stayed away from real axis that have better rate capacity. Due to faster kinetic diffusion processes, ZM-2 presented a slow specific capacitance decrease with increased current densities. The equivalent series resistance (R_e) of ZM-2 was the lowest, resulting from good dynamic diffusion performance. As mentioned above, as the MnO_2 content in nanosheets increased, the electrochemical reaction of the electrode was promoted. Because the composite provided more active sites and ion/electron transport channels, reducing internal resistance and promoting rate capability. Thus, the composite R_e was smaller than pure $ZnCo_2O_4$, but only very small amount of MnO_2 went into contact with the electrolyte and the excess MnO_2 would agglomerate to prevent the transfer of ion/electron [36, 37]. From these two

figures, we could see that the composite electrochemical performance was much better than the pure $ZnCo_2O_4$, and MnO_2 at a concentration of 0.031 g to achieve the best.

To clearly demonstrate the practical performance of as-prepared $ZnCo_2O_4/MnO_2$ nanosheets electrode, an asymmetric supercapacitor (ASC) was fabricated, in which ZM-2 and active carbon were used to be positive and negative electrodes, respectively. The cyclic voltammograms in Fig. 9a was carried out to evaluate the ASC potential windows. The unchanged shape of CV curves indicated that the super-capacitor achieved a 1.5 V stable voltage window at a mutative scan rate of 5–100 mV/s. Figure 9b was the GCD curves of ASC, displaying ideal triangular and symmetric shapes that implies excellent reversibility. Specific capacitance ranged from 54.2 to 36.13 F/g at a variable current density of 1–10 A/g. Figure 9c showed that the Ragone plots of the ASC were calculated from GCD curves, the obtained maximum energy density 16.94 W h/kg (a power density of 750 W/kg) and maximum power density 7500 W/kg (an energy density of 11.3 W h/kg) due to the high specific capacitance and additional electronic transmission channels. The composite material of $ZnCo_2O_4$ and MnO_2 as the electrode of the supercapacitor showed significantly better power density and energy density than reported literatures [38, 39]. To better understand the electrochemical performance of $ZnCo_2O_4/MnO_2$ nanosheets in such a hybrid electrode compared to other related researches, the corresponding data were listed in Table 1. Cycle stability testing was another fundamental feature of a high-performance ASC and measured the device's capacitance during charge–discharge cycles at 1 A/g after 1500 cycles. Here, the capacitance of the ASC retained 98.5% of its initial value in Fig. 9d. The potential application of ZM-2 in super-capacitor was further demonstrated by a setup which connected two ASC devices to give electrical power for a commercial LED bulb belt (Fig. 9d, inset), explaining that the assembled ASC device possessed a great prospect in practical energy storage.

4 Conclusions

To sum up, the $ZnCo_2O_4/MnO_2$ nanosheets composite had been successfully synthesized. The as-prepared composition exhibited a better specific capacity of 286 F/g. In addition, an ASC device, based on $ZnCo_2O_4/MnO_2$, was well designed, exhibiting a maximum energy density of 16.94 W h/kg and a maximum power density of 7500 W/kg. This $ZnCo_2O_4/MnO_2$-based ASC system had superior cycling stability (98.5% capacitance retention after 1500 cycles). The device could easily light a commercial LED bulb belt, endowing

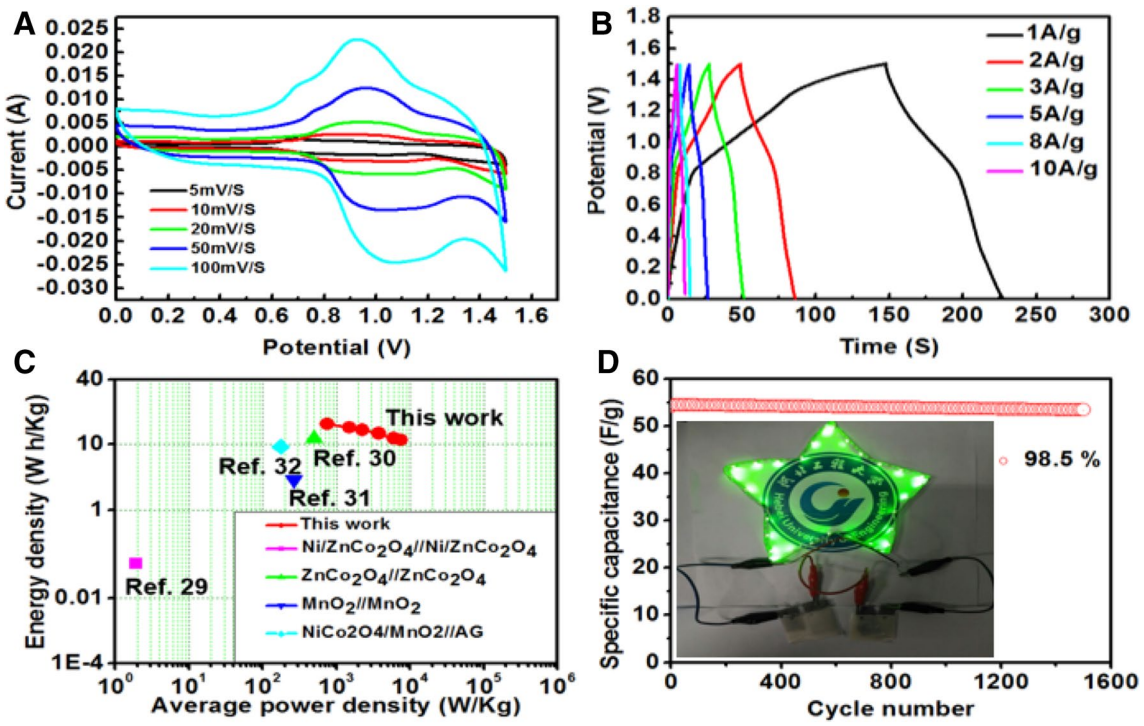

Fig. 9 Electrochemical performance of the asymmetric supercapacitor based on the ZM-2 and AC as positive and negative electrodes: **a** The CV curves of the ASC device in different scan rate. **b** Galvanostatic charge–discharge curves at different current densities from 1 to 10 A/g. **c** Comparison with the related references in the Ragone plots in which energy density versus power density. **d** Cycling performance after 1500 cycles at 1 A/g of the asymmetric supercapacitor (insert photograph showing a green LED belt was powered by ASC devices)

Table 1 The comparison of the electrochemical performance for the composite electrode in our work and other reported electrodes

Electrode materials	Capacitance (F/g)	Energy density (Wh/Kg)	Power density (W/Kg)	Capacitance retention (%)	Cycle number	References
3D graphene/MnO_2	29.8 (1.5 mA/cm^2)	6.8	2500	93.28	500	[40]
Graphite/PEDOT/MnO_2	20.8 (1 A/g)	31.4		81.1	2000	[41]
Ultrathin porous MnO_2 nanoflowers	85.8 (200 mA/g)	47.4	2000	90	1000	[42]
$ZnCo_2O_4$/CC	423 (2 mA/cm^2)	12.5	3600	96.2	1000	[43]
$ZnCo_2O_4$/Ni	10.9 (10 mV/S)	0.076	1.9	92	3500	[44]
This work	54.2 (1 A/g)	16.94	7500	98.5	1500	

the ASC has new opportunities as energy storage devices. The excellent electrochemical performance might ascribed to the excellent conductive substrate of $ZnCo_2O_4$ covered by high capacity of MnO_2, in addition, the nanosheets structure provided more active sites that contributed to the attachment of MnO_2, offering fast transmission channels for electron. The synergetic effect between $ZnCo_2O_4$ and MnO_2 result in that the entire system has superior electrochemical performance. The $ZnCo_2O_4/MnO_2$ nanosheets composite with these favorable electrochemical properties may provide reliable electrode materials for super-capacitors in the future.

Acknowledgements The authors acknowledge the financial support of the National Natural Science Foundation of China (Grant nos. 51402082), the Natural Science Foundation of Hebei Province (Grant no. E2015402058).

References

1. Y. Liu, D. Yan, R.F. Zhuo et al., Design, hydrothermal synthesis and electrochemical properties of porous birnessite-type manganese dioxide nanosheets on graphene as a hybrid material for supercapacitors. J. Power Sour. **242**(22), 78–85 (2013)
2. T. Cottineau, M. Toupin, T. Delahaye et al., Nanostructured transition metal oxides for aqueous hybrid electrochemical supercapacitors. Appl. Phys. A Mater. Sci. Process. **82**(4), 599–606 (2006)
3. A. Balducci, F. Soavi, M. Mastragostino et al., The use of ionic liquids as solvent-free green electrolytes for hybrid supercapacitors. Appl. Phys. A Mater. Sci. Process. **82**(4), 627–632 (2006)
4. Y.Q. Zhu, C.B. Cao, J.T. Zhang et al., Two-dimensional ultrathin $ZnCo_2O_4$ nanosheets: general formation and lithium storage application. J. Mater. Chem. A **3**(18), 9556–9564 (2015)
5. K.W. Qiu, Y. Lu, D.Y. Zhang et al., Mesoporous, hierarchical core/shell structured $ZnCo_2O_4/MnO_2$ nanocone forests for high-performance supercapacitors. Nano Energy **11**, 687–696 (2015)
6. H. Jiang, C.Z. Li, T. Sun et al., High-performance supercapacitor material based on $Ni(OH)_2$ nanowire-MnO_2 nanoflakes core-shell nanostructures. Chem. Commun. **48**(20), 2606–2608 (2012)
7. M. Huang, Y.X. Zhang, F. Li et al., Self-assembly of mesoporous nanotubes assembled from interwoven ultrathin birnessite-type MnO_2 nanosheets for asymmetric supercapacitors. Sci. Rep. **4**(4), 3878–3885 (2014)
8. A.L.M. Reddy, M.M. Shaijumon, S.R. Gowda et al., Multisegmented Au-MnO_2/carbon nanotube hybrid coaxial arrays for high-power supercapacitor applications. J. Phys. Chem. C **117**(42), 658–663 (2010)
9. J. Di, X.C. Fu, H.J. Zheng et al., H–TiO_2/C/MnO_2, nanocomposite materials for high-performance supercapacitors. J. Nanoparticle Res. **17**(6), 255–266 (2015)
10. Z. Yu, C. Li, D. Abbitt et al., Flexible, sandwich-like Ag-nanowire/PEDOT:PSS-nanopillar/MnO_2 high performance supercapacitors. J. Mater. Chem. A. **2**(28), 10923–10929 (2014)
11. G.H. Yu, L.B. Hu, N. Liu et al., Enhancing the supercapacitor performance of graphene/MnO_2 nanostructured electrodes by conductive wrapping. Nano Lett. **11**(10), 4438–4442 (2011)
12. S. Chen, J.W. Zhu, X.D. Wu et al., Graphene oxide–MnO_2 nanocomposites for supercapacitors. Acs Nano. **4**(5), 2822–2830 (2010)
13. M. Huang, F. Li, F. Dong et al., MnO_2-based nanostructures for high-performance supercapacitors. J. Mater. Chem. A **3**(43), 21380–21423 (2015)
14. B. Mendoza-Sánchez, Y. Gogotsi, Synthesis of two-dimensional materials for capacitive energy storage. Adv. Mater. **28**(29), 6104–6135 (2016)
15. H. Fan, X. Huang, L. Shang et al., Controllable synthesis of ultrathin transition-metal hydroxide nanosheets and their extended composite nanostructures for enhanced catalytic activity in the heck reaction. Angew. Chem. Int. Edit. **128**(6), 2167–2170 (2016)
16. D. Rangappa, K.D. Murukanahally, T. Tomai et al., Ultrathin nanosheets of Li_2MSiO_4 (M = Fe, Mn) as high-capacity Li-ion battery electrode. Nano Lett. **12**(3), 1146–1151 (2012)
17. Y.Q. Zhu, C.B. Cao, T. Shi et al., Ultrathin nickel hydroxide and oxide nanosheets: synthesis, characterizations and excellent supercapacitor performances. Sci. Rep. **4**, 5787–5793 (2014)
18. J. Yan, Z.J. Fan, W. Sun et al., Advanced asymmetric supercapacitors based on $Ni(OH)_2$/graphene and porous graphene electrodes with high energy density. Adv. Funct. Mater. **22**(12), 2632–2641 (2012)
19. Y.M. Lv, A.F. Liu, H.W. Che et al., Three-dimensional interconnected $MnCo_2O_4$ nanosheets@$MnMoO_4$ nanosheets core-shell nanoarrays on Ni foam for high-performance supercapacitors. Chem. Eng. J. **336**, 64–73 (2018)
20. Y.Z. Su, K. Xiao, N. Li et al., Amorphous $Ni(OH)_2$@three-dimensional Ni core-shell nanostructures for high capacitance pseudocapacitors and asymmetric supercapacitors. J. Mater. Chem. A. **2**(34), 13845–13853 (2014)
21. G.F. Chen, Z.Q. Liu, J.M. Lin et al., Hierarchical polypyrrole based composites for high performance asymmetric supercapacitors. J. Power Sour. **283**, 484–493 (2015)
22. H.W. Che, Y.M. Lv, A.F. Liu et al., Facile synthesis of three dimensional flower-like Co_3O_4@MnO_2 core-shell microspheres as high-performance electrode materials for supercapacitors. Ceram. Int. **43**(8), 6054–6062 (2017)
23. D. Ma, J. Cai, X.X. Wu et al., Treatment of multiwall carbon nanotubes based on the modified Hummers method for supercapacitor electrode materials. J. Renew. Sustain. Energy **8**(1), 1972–1981 (2016)

24. Y.M. Lv, H.W. Che, A.F. Liu et al., Urchin-like α-FeOOH@MnO_2 core–shell hollow microspheres for high-performance supercapacitor electrode. J. Appl. Electrochem. **47**(4), 433–444 (2017)
25. H.P. Yang, J. Jiang, W.W. Zhou et al., Influences of graphene oxide support on the electrochemical performances of graphene oxide-MnO_2 nanocomposites. Nanoscale Res. Lett. **6**(1), 531–538 (2011)
26. X.B. Zhong, H.Y. Wang, Z.Z. Yang et al., Facile synthesis of mesoporous $ZnCo_2O_4$, coated with polypyrrole as an anode material for lithium-ion batteries. J. Power Sour. **296**, 298–304 (2015)
27. Z.S. Wu, W. Ren, D.W. Wang et al., High-Energy MnO_2 nanowire/graphene and graphene asymmetric electrochemical capacitors. Acs Nano. **4**(10), 5835–5842 (2010)
28. B.K. Guan, D. Guo, L.L. Hu et al., Facile synthesis of $ZnCo_2O_4$ nanowire cluster arrays on Ni foam for high-performance asymmetric supercapacitors. J. Mater. Chem. A **2**(38), 16116–16123 (2014)
29. L.Y. Yuan, X.H. Lu, X. Xiao et al., Flexible solid-state supercapacitors based on carbon nanoparticles/MnO_2 nanorods hybrid structure. Acs Nano. **6**(1), 656–661 (2012)
30. M.J. Chen, J.Y. Wang, H.J. Tang et al., Synthesis of multi-shelled MnO_2 hollow microspheres via an anion-adsorption process of hydrothermal intensification. Inorg. Chem. Front. **3**(8), 1065–1070 (2016)
31. T.F. Hung, S.G. Mohamed, C.C. Shen et al., Mesoporous $ZnCo_2O_4$ nanoflakes with bifunctional electrocatalytic activities toward efficiencies of rechargeable lithium-oxygen batteries in aprotic media. Nanoscale. **5**(24), 12115–12119 (2013)
32. Y.M. Guan, Z.C. Guo, H.W. Che et al., Core/shell nanorods of MnO_2/carbon embedded with Ag nanoparticles as high-performance electrode materials for supercapacitors. Chem. Eng. J. **331**(1), 23–30 (2018)
33. W.B. Fu, Y.L. Wang, W.H. Han et al., Construction of hierarchical $ZnCo_2O_4$@$Ni_xCo_{2x}(OH)_{6x}$ core/shell nanowire arrays for high-performance supercapacitors. J. Mater. Chem. A. **4**(1), 173–182 (2015)
34. J. Yan, Z.J. Fan, T. Wei et al., Fast and reversible surface redox reaction of graphene–MnO_2, composites as supercapacitor electrodes. Carbon **48**(13), 3825–3833 (2010)
35. M. Huang, X.L. Zhao, F. Li et al., Facile synthesis of ultrathin manganese dioxide nanosheets arrays on nickel foam as advanced binder-free supercapacitor electrodes. J. Power Sour. **277**, 36–43 (2015)
36. D.Y. Yu, Z.Q. Zhang, Y.N. Meng et al., The synthesis of hierarchical $ZnCo_2O_4$@MnO_2 core–shell nanosheet arrays on nickel foam for high-performance all-solid-state asymmetric supercapacitors. Inorg. Chem. Front. **5**(3), 597–604 (2018)
37. W. Ma, H. Nan, Z. Gu et al., Superior performance asymmetric supercapacitors based on $ZnCo_2O_4$@MnO_2 core–shell electrode. J. Mater. Chem. A **3**(10), 5442–5448 (2015)
38. J.A. Rajesh, B.K. Min, J.H. Kim et al., Cubic spinel AB_2O_4 type porous $ZnCo_2O_4$ microspheres: facile hydrothermal synthesis and their electrochemical performances in pseudocapacitor. J. Electrochem. Soc. **163**(10), A2418–A2427 (2016)
39. M. Kuang, Z.Q. Wen, X.L. Guo et al., Engineering firecracker-like beta-manganese dioxides@spinel nickel cobaltates nanostructures for high-performance supercapacitors. J. Power Sour. **270**(4), 426–433 (2014)
40. Y.M. He, W.J. Chen, X.D. Li et al., Freestanding three-dimensional graphene/MnO_2 composite networks as ultralight and flexible supercapacitor electrodes. Acs Nano **7**(1), 174–182 (2013)
41. P.Y. Tang, L.J. Han, L. Zhang, Facile synthesis of graphite/PEDOT/MnO_2 composites on commercial supercapacitor separator membranes as flexible and high-performance supercapacitor electrodes. Acs Appl. Mater. Interfaces **6**(13), 10506–10515 (2014)
42. H. Jiang, C.Z. Li, T. Sun et al., A green and high energy density asymmetric supercapacitor based on ultrathin MnO_2 nanostructures and functional mesoporous carbon nanotube electrodes. Nanoscale. **4**(3), 807–812 (2012)
43. S.J. Patil, J. Park, D.W. Lee, Facial synthesis of nanostructured $ZnCo_2O_4$ on carbon cloth for supercapacitor application. IOP Conf. Ser. Mater. Sci. Eng. **282**(1), 012004 (2017)
44. H. Wu, Z. Lou, H. Yang et al., A flexible spiral-type supercapacitor based on $ZnCo_2O_4$ nanorod electrodes. Nanoscale **7**(5), 1921–1926 (2015)